

Curvature approximation on surfaces – A Discrete Exterior Calculus Approach

I. Nitschke¹, A. Voigt^{1,2}

Abstract

Lorem ipsum dolor sit amet, consetetur sadipscing elitr, sed diam nonumy eirmod tempor invidunt ut labore et dolore magna aliquyam erat, sed diam voluptua. At vero eos et accusam et justo duo dolores et ea rebum. Stet clita kasd gubergren, no sea takimata sanctus est Lorem ipsum dolor sit amet. Lorem ipsum dolor sit amet, consetetur sadipscing elitr, sed diam nonumy eirmod tempor invidunt ut labore et dolore magna aliquyam erat, sed diam voluptua. At vero eos et accusam et justo duo dolores et ea rebum. Stet clita kasd gubergren, no sea takimata sanctus est Lorem ipsum dolor sit amet. Lorem ipsum dolor sit amet, consetetur sadipscing elitr, sed diam nonumy eirmod tempor invidunt ut labore et dolore magna aliquyam erat, sed diam voluptua. At vero eos et accusam et justo duo dolores et ea rebum. Stet clita kasd gubergren, no sea takimata sanctus est Lorem ipsum dolor sit amet.

Keywords: Surfaces, Curvature, DEC

1. Introduction

Lorem ipsum dolor sit amet, consetetur sadipscing elitr, sed diam nonumy eirmod tempor invidunt ut labore et dolore magna aliquyam erat, sed diam voluptua. At vero eos et accusam et justo duo dolores et ea rebum. Stet clita kasd gubergren, no sea takimata sanctus est Lorem ipsum dolor sit amet. Lorem ipsum dolor sit amet, consetetur sadipscing elitr, sed diam nonumy eirmod tempor invidunt ut labore et dolore magna aliquyam erat, sed diam voluptua. At vero eos et accusam et justo duo dolores et ea rebum. Stet clita kasd gubergren, no sea takimata sanctus est Lorem ipsum dolor sit amet. Lorem ipsum dolor sit amet, consetetur sadipscing elitr, sed diam nonumy eirmod tempor invidunt ut labore et dolore magna aliquyam erat, sed diam voluptua. At vero eos et accusam et justo duo dolores et ea rebum. Stet clita kasd gubergren, no sea takimata sanctus est Lorem ipsum dolor sit amet. Lorem ipsum dolor sit amet, consetetur sadipscing elitr, sed diam nonumy eirmod tempor invidunt ut labore et dolore magna aliquyam erat, sed diam voluptua. At vero eos et accusam et justo duo dolores et ea rebum. Stet clita kasd gubergren, no sea takimata sanctus est Lorem ipsum dolor sit amet.

2. Discrete Exterior Calculus (DEC)

The Discrete Exterior Calculus [13, 8] defines discrete differential p -forms on a triangulated mesh (simplicial complex). For surface meshes, i.e. triangulated orientable 2-manifolds, the degree of the discrete p -forms is 0, 1 or 2 and they are represented by scalars on vertices, edges, triangles or chains of them. Operators for the differential forms, like the exterior derivation \mathbf{d} or the hodge star \star ,

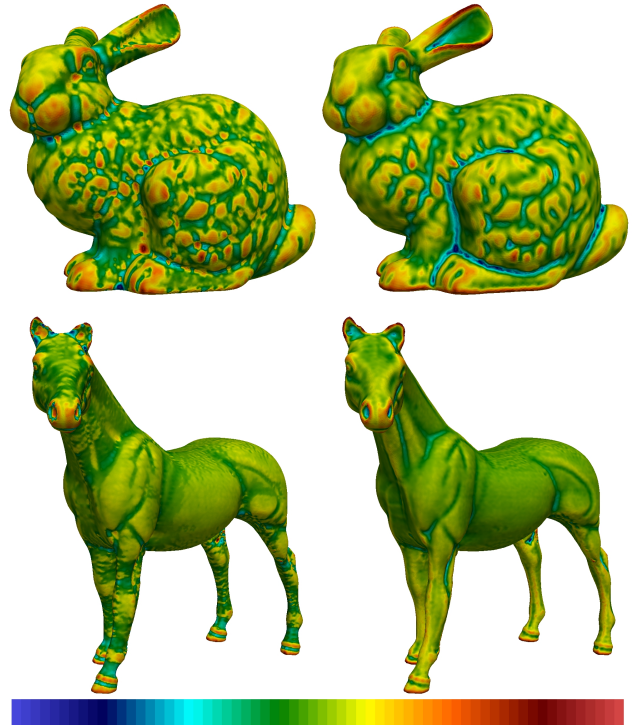


Figure 1: Surface curvature approximations of the Stanford Bunny (39998 DOFs) and a horse (89983 DOFs). Left: Gaussian curvature K (square root scaled colours). Right: Mean curvature H (linear scaled colours)

Email addresses: ingo.nitschke@tu-dresden.de (I. Nitschke), axel.voigt@tu-dresden.de (A. Voigt)

¹Department of Mathematics, TU Dresden, 01062 Dresden, Germany

²Center of Advanced Modeling and Simulation, TU Dresden, 01062 Dresden, Germany

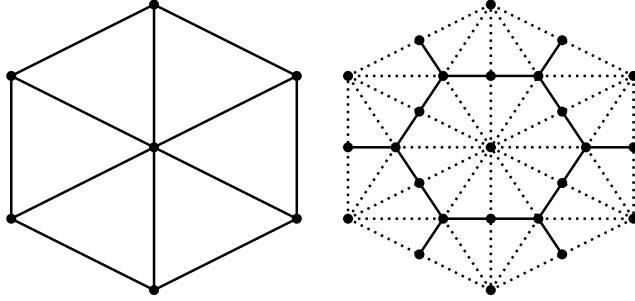


Figure 2: Example of a circumcenter subdivision. Left: A primal mesh K . Right: The resultant dual mesh $\text{csd}K$. All new vertices are the circumcenters of the triangles and edges. The solid lines highlights the edges of the Voronoi mesh $\star K \leq \text{csd}K$.

can be approximated by expressions on the discrete geometrical structure. E.g. the integral over a triangle of the exterior derivation \mathbf{d} for a 1-form can be expressed as the integral of this 1-form over the boundaries edges of the triangle. This follows directly from the Stokes Theorem [1, Ch. 7].

2.1. Discrete manifolds

In our setting, the surface meshes are linear triangulations of orientable closed 2-manifolds. Such a Triangulation are sets of p -simplices $\{\sigma^p\}$ of the same degree p , e.g. sets of vertices, edges and triangles, and form a simplicial complex of dimension $n = 2$. A simplicial complex K comply two essential rules:

1. Every face of a simplex $\sigma^p \in K$ is in K .
2. The intersection of two simplices in K is either in K or empty.

We shortly write $\sigma^q \prec \sigma^p$ (or $\sigma^p \succ \sigma^q$), iff $q < p$ and σ^q is a face of σ^p . It is required, that the polytop

$$|K| := \bigcup_{\sigma \in K} \sigma \quad (1)$$

of K is a C^0 -manifold and we call K a manifold-like simplicial complex. For a higher consistence to the smooth model, we assume that the simplicial complex is orientable, i.e. all triangles $\sigma^2 \in K$ have the same orientation. The orientation of a triangle is define as one of the two equivalence classes, that arise from the kind of counting the vertices (clockwise or counterclockwise). We write $\sigma^2 = [v_0, v_1, v_2]$ to mark the order of the vertices v_i . In the same manner a edge $\sigma^1 = [v_0, v_1]$ get an declared orientation. Such a manifold-like orientable simplicial complex is called a primal mesh.

For the existence of a dual mesh, we also need, that the primal mesh is well-centered, i.e. for all triangles $\sigma^2 \in K$ the circumcenter $c(\sigma^2)$ lies in the interior of σ^2 . A dual mesh $\text{csd}K$ is the circumcenter subdivision of a well-centered primal mesh K . For a explanatory example see figure 2. The dual mesh is also a primal mesh, but it is not well-centered.

2.2. Chains

An important role in the DEC are chains. A p -chain is the formal sum of p -simplices with coefficients in \mathbb{Z} . Therewith, we denote the space of all p -chains of K by

$$C_p(K) := \left\{ \sum_{\sigma \in K^{(p)}} a_\sigma \sigma \mid a_\sigma \in \mathbb{Z} \right\}. \quad (2)$$

$K^{(p)}$ is the set of all p -simplices of K . For chains we can use the universal property, because $C_p(K)$ is a free abelian group with the generating set $K^{(p)}$. Hence, the diagram

$$\begin{array}{ccc} C_p(K) & & (3) \\ \downarrow & \searrow \widehat{op} & \\ K^{(p)} & \xrightarrow{op} & \mathfrak{A} \end{array}$$

commutes for a arbitrary abelian group \mathfrak{A} and homomorphism $op = \widehat{op}|_{K^{(p)}}$ and \widehat{op} is unique determinated by op , i.e. it is quit enough to define operators for chains only on the simplices.

2.3. Geometrical operators

The two momentous operators on chains are the boundary operator ∂ and the star operator \star . These are the geometrical tools for the discrete exterior derivation \mathbf{d} resp. the discrete Hodge star $*$, what we will see below.

2.3.1. The star operator

For a general definition of the star operator \star see [13, 8] or [9, Ch. 7]. In our two dimensional well-centered primal mesh case it is enough to define the star operator $\star : C_p(K) \rightarrow C_{2-p}(\text{csd}K)$ by

$$\star \sigma^0 := \sum_{\sigma^0 \prec \sigma^1 \prec \sigma^2} s_{\sigma^1 \sigma^2} [\sigma^0, c(\sigma^1), c(\sigma^2)] \quad (4)$$

$$\star \sigma^1 := \sum_{\sigma^1 \prec \sigma^2} s_{\sigma^2} [c(\sigma^1), c(\sigma^2)] \quad (5)$$

$$\star \sigma^2 := c(\sigma^2) \quad (6)$$

The factors s_{\bullet} are signs to prevent orientation properties, like the orientability of the dual mesh. (4) describe the Voronoi cell of the primal vertex σ^0 , (5) describe the Voronoi edge of the primal edge σ^1 (c.p. figure 2) and (6) describe the Voronoi vertex of a primal triangle σ^2 . With the notation $C_{2-p}(\star K)$ for the image of \star , the star operator, act on $C_{2-p}(\star K)$ and map to $C_p(K)$, is for $p = 0, 2$ simply the inverse. For $p = 1$ we must swap the orientation, i.e. $\star \star \sigma^1 = -\sigma^1$.

2.3.2. The boundary operator

Let K be a primal mesh (not necessary well-centered). The boundary operator $\partial : C_p(K) \rightarrow C_{p-1}(K)$ is defined

by

$$\partial\sigma^p := \begin{cases} \sum_{i=0}^p (-1)^i [v_0, v_1, \dots, \hat{v}_i, \dots, v_p] & \text{for } p = 1, 2 \\ 0 & \text{for } p = 0 \end{cases} \quad (7)$$

(\hat{v}_i is omitted) and comply the property $\partial \circ \partial = 0$. This is the authorization to call the sequence $(C_p(K), \partial)$ (and also $(C_p(\star K), \partial)$)

$$\begin{array}{ccccccc} 0 & \longrightarrow & C_2(K) & \xrightarrow{\partial} & C_1(K) & \xrightarrow{\partial} & C_0(K) \longrightarrow 0 \\ & & \uparrow \ast & & \uparrow \ast & & \uparrow \ast \\ 0 & \longleftarrow & C_0(\star K) & \xleftarrow[\partial]{} & C_1(\star K) & \xleftarrow[\partial]{} & C_2(\star K) \longleftarrow 0 \end{array} \quad (8)$$

a chain complex.

2.4. Discrete differential forms

A discrete p -form α is a homomorphism from the chain group $C_p(K)$ to the additive group \mathbb{R} . Thus, the space of discrete p -form is the space of cochains $\text{Hom}(C_p(K), \mathbb{R})$, denoted as $C^p(K)$ or, under attention the analogy to smooth differential forms, $\Omega_d^p(K)$. The crucial map, that define such homomorphisms and give the relation to the smooth forms, is the de Rham map

$$\begin{aligned} \psi : \Omega^p(M) &\rightarrow C^p(L) = \Omega_d^p(L) \\ \alpha &\mapsto \left(\sigma^p \mapsto \int_{\sigma^p} \alpha =: \langle \psi(\alpha), \sigma^p \rangle \right). \end{aligned} \quad (9)$$

The right hand side is the pairing notation, which we want to use. At this, L is the abstract simplicial complex of K and arise if all simplices from K are projected to the underlying manifold M , i.e. $|L| = M$ and $L = \pi(K)$ with a projection map $\pi : |K| \rightarrow M$. But the projection and in the most cases the manifold M is not exactly known, so for interest of simplification we can approximate the integral in (9) with a linear quadrature I on the vertices of a given simplex $\sigma^p \in K$:

$$\langle \psi(\alpha), \pi(\sigma^p) \rangle \approx I_{\sigma^p}(\alpha). \quad (10)$$

For $p = 0$ and a function (0-form) $f : M \rightarrow \mathbb{R}$ and a vertex (0-simplex) is this exact, i.e.

$$\langle \psi(f), \pi(v) \rangle = \langle \psi(f), v \rangle = f(v). \quad (11)$$

For $p > 1$ the question about evaluating the integral in (9) is pure formal in this paper, because in all of our computation, we can reduce the problems to scalar valued formulations. Henceforth, the projection π is omitted in the pairing notation, i.e. we write $\langle \psi(\alpha), \sigma^p \rangle$ instead of $\langle \psi(\alpha), \pi(\sigma^p) \rangle$.

2.5. DEC operators

For the definition of a discrete version of the Hodge star $*$ or the exterior derivative \mathbf{d} we can fall back to the geometric operators.

2.5.1. The discrete Hodge star operator

The discrete Hodge star $* : \Omega_d^p(K) \rightarrow \Omega_d^{2-p}(*K)$ is nothing more than scale the evaluation of a discrete p -form by the ratio of the dual (Voronoi) and the primal volumes.

$$\langle * \alpha, * \sigma^p \rangle := \frac{|* \sigma^p|}{|\sigma^p|} \langle \alpha, \sigma^p \rangle \quad (12)$$

for a simplex $\sigma^p \in K$ and a $\alpha \in \Omega_d^p(K)$. Note that the intrinsic volume of a 0-simplex is 1. (In [16] we can see that (12) is consistent with $\mathcal{O}(h^{3-p})$ for the maximum circumscribed diameter h .) The discrete Hodge star on a discrete dual form $\hat{\alpha} \in \Omega_d^p(*K)$ can be obtained implicitly by the rule $* * \hat{\alpha} = (-1)^p \hat{\alpha}$, which holds on a even-dimensional simplicial complex as well as for smooth forms on a even-dimensional manifold.

2.5.2. The discrete exterior derivative

The main advantage in the definition of discrete differential forms as integral evaluation of smooth forms on (abstract) simplices is that we are able to use the Stokes theorem (14) to describe a discrete exterior derivative $\mathbf{d} : \Omega_d^p(K) \rightarrow \Omega_d^{p+1}(K)$:

$$\langle \mathbf{d}\psi(\alpha), \sigma^p \rangle := \langle \psi(\mathbf{d}\alpha), \sigma^p \rangle \quad (13)$$

$$= \langle \psi(\alpha), \partial\sigma^p \rangle \quad (14)$$

(this applies on $\star K$ also) and there is no approximation error accept the interpretation of the integral expression. Hence, the discrete exterior derivative inherit the complex property of the boundary operator, i.e. $\mathbf{d} \circ \mathbf{d} = 0$. That's why the sequence of discrete differential forms (cochains) $(\Omega_d^p(K), \mathbf{d})$ (and $(\Omega_d^p(\star K), \mathbf{d})$)

$$\begin{array}{ccccccc} 0 & \longrightarrow & \Omega_d^0(K) & \xrightarrow{\mathbf{d}} & \Omega_d^1(K) & \xrightarrow{\mathbf{d}} & \Omega_d^2(K) \longrightarrow 0 \\ & & \uparrow \ast & & \uparrow \ast & & \uparrow \ast \\ 0 & \longleftarrow & \Omega_d^2(\star K) & \xleftarrow[\mathbf{d}]{} & \Omega_d^1(\star K) & \xleftarrow[\mathbf{d}]{} & \Omega_d^0(\star K) \longleftarrow 0 \end{array} \quad (15)$$

is a cochain complex.

2.5.3. The discrete Laplace-Beltrami operator

The Laplace-Beltrami operator $\Delta_B = * \mathbf{d} * \mathbf{d}$ is the special case of the negative Laplace-de Rham operator $-\Delta_{dR} = * \mathbf{d} * \mathbf{d} + \mathbf{d} * \mathbf{d} *$ for 0-forms on a 2-manifold or in general on a even-dimensional manifold. To discretize Δ_B all of work is done above, because we can use the definitions (12) and (13) step by step in the same manner

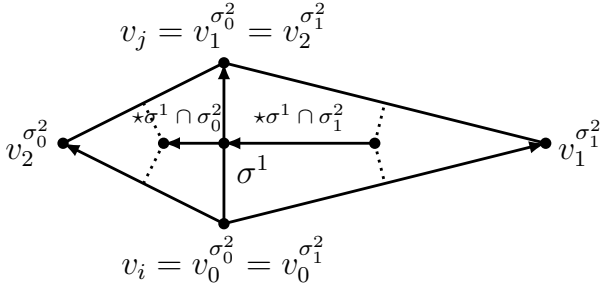


Figure 3: Two adjacent (triangle) elements share a common edge $\sigma^1 = [v_i, v_j]$. The vertices are local indexed on these elements.

like the smooth exterior calculus. I.e. for a 0-form f on a vertex v it results in

$$\langle \Delta_B f, v \rangle = \frac{1}{|\star v|} \sum_{\sigma^1=[v, v_i] \in K} \frac{|\star \sigma^1|}{|\sigma^1|} (f(v_i) - f(v)). \quad (16)$$

For greater details see [13] or [8]. (16), equivalent to the cotan-formular described in [15], is a approximation of order 2 (see [24]) and was already earlier published in [19] as a non-DEC consequence.

Note on Implementation. In section 3.1 we need the discrete Laplace-Beltrami operator to approximate the mean curvature. One way to do that is to represent the discrete linear operators $*$ and \mathbf{d} as matrices act on a vector of all vertices, edges or triangles. So the discrete Laplace-Beltrami is nothing more than the product of these matrices (see [10], [2] or [6]).

A more “FEM-like” manner is to decompose (16) in parts, which can be computed on all (triangle) elements without knowledge of their neighbours. For this we formulate the operator on the Voronoi cells to cancel the scale factor $|\star v|^{-1}$ in (16), split the sum and use a local vertex indexing on all elements:

$$\langle * \Delta_B f, \star v_i \rangle = \sum_{\sigma^1=[v_i, v_j]} \frac{|\star \sigma^1|}{|\sigma^1|} (f(v_j) - f(v_i)) \quad (17)$$

$$= \sum_{\sigma^2=\left[v_0^{\sigma^2}, v_1^{\sigma^2}, v_2^{\sigma^2}\right]} \sum_{l=1,2} C_{0,l}^{\sigma^2} (f_l^{\sigma^2} - f_0^{\sigma^2}). \quad (18)$$

$f_l^{\sigma^2} \in \mathbb{R}$ are the evaluations of f on the local vertices $v_l^{\sigma^2}$ of the element σ^2 . Figure 3 clarify this setting. The coefficients $C_{0,l}^{\sigma^2} \in \mathbb{R}$ are generally defined by

$$C_{k,l}^{\sigma^2} := C_{l,k}^{\sigma^2} := \frac{|\star [v_k^{\sigma^2}, v_l^{\sigma^2}] \cap \sigma^2|}{|[v_k^{\sigma^2}, v_l^{\sigma^2}]|}. \quad (19)$$

Hence we can extract from (18) a local coefficients matrix

$$A^{\sigma^2} := \begin{bmatrix} - (C_{01}^{\sigma^2} + C_{02}^{\sigma^2}) & C_{01}^{\sigma^2} & C_{02}^{\sigma^2} \\ C_{01}^{\sigma^2} & - (C_{01}^{\sigma^2} + C_{12}^{\sigma^2}) & C_{12}^{\sigma^2} \\ C_{02}^{\sigma^2} & C_{12}^{\sigma^2} & - (C_{02}^{\sigma^2} + C_{12}^{\sigma^2}) \end{bmatrix} \quad (20)$$

which holds all computation parts for the local vertices. All A^{σ^2} can be assembly in a familiar way to get a sparse global matrix $A \in \mathbb{R}^{N_{\sigma^0} \times N_{\sigma^0}}$, where N_{σ^0} are the number of vertices in K . At the end, for $f_h \in \mathbb{R}^{N_{\sigma^0}}$, the vector of evaluations for f (resp. vector of DOFs³), Af_h is the result of (17) on all global vertices.

The great advantage of this proceeding is the compatibility to existing Finite Element code like AMDiS⁴ [23]. Only the element operator A^{σ^2} must be implemented under use of linear test functions for the interpolation. All other works, like mesh management, problem formulation on the user level, assembling and solving of the linear System, can be done by the FE-toolbox.

2.5.4. The discrete gradient

The gradient of a scalar valued function f can be obtained by rising the indices of its exterior derivative, in other words $\nabla f = (\mathbf{d}f)^\sharp$. Unfortunately, the sharp operator \sharp depends on the (unknown) metric of the manifold. In [13] it is suggested to use the following discrete sharp operator for such a exact 1-form $\mathbf{d}f$ to get a discrete gradient:

$$\langle (\mathbf{d}f)^\sharp, \star \sigma^2 \rangle := \sum_{\sigma^0 \prec \sigma^2} (f(\sigma^0) - f(w)) \nabla_{\mathbb{R}^3} \Phi_{\sigma^0}^{\sigma^2}, \quad (21)$$

with a arbitrary vertex $w \prec \sigma^2$, $\Phi_{\sigma^0}^{\sigma^2}$ is the linear test function (hat function) for the vertex σ^0 restricted to σ^2 and $\nabla_{\mathbb{R}^3}$ is the usual \mathbb{R}^3 gradient in the ambient space. The formulation for the \mathbb{R}^3 vector $(\mathbf{d}f)^\sharp$ is to read component wise as a \mathbb{R}^3 -vectorized scalar formulation. (21) gives us a tangential vector of the polytop $|K|$ on the circumcenter of the triangle σ^2 . But in our setting we want to use a gradient on a vertex of the primal mesh, resp. interpreted on the associated Voronoi cell. A simple way to get such a discrete gradient, is to average (21) over all dual vertices of the Voronoi cell related to the primal vertex v :

$$\langle * \bar{\nabla} f, \star v \rangle = \sum_{\sigma^2 \succ v} |\star v \cap \sigma^2| \sum_{\sigma^0 \prec \sigma^2} (f(\sigma^0) - f(v)) \nabla_{\mathbb{R}^3} \Phi_{\sigma^0}^{\sigma^2} \quad (22)$$

The drawback of the discrete average gradient, which we will use in section 3.2, is that $|K|$ has no tangential space on its vertices, because the polytop is not continuous differentiable in v . This makes the situation for a numerical analysis slightly difficult. But comparing calculations for several manifolds and functions and the results in section 4 indicate the consistence of (22) to the smooth gradient, if the triangulation is fine enough.

³Degree Of Freedom

⁴Adaptive MultiDimensional Simulation toolbox, developed at Institute for Scientific Computing, TU-Dresden

Note on Implementation. Like in section 2.5.3, we can deploy a coefficients matrix for the q -th component of (22) for a triangle σ^2 :

$$\begin{bmatrix} -\left(C_{01q}^{\sigma^2} + C_{02q}^{\sigma^2}\right) & C_{01q}^{\sigma^2} & C_{02q}^{\sigma^2} \\ C_{10q}^{\sigma^2} & -\left(C_{10q}^{\sigma^2} + C_{12q}^{\sigma^2}\right) & C_{12q}^{\sigma^2} \\ C_{20q}^{\sigma^2} & C_{21q}^{\sigma^2} & -\left(C_{20q}^{\sigma^2} + C_{21q}^{\sigma^2}\right) \end{bmatrix} \quad (23)$$

with

$$C_{klq}^{\sigma^2} := |\star v_k^{\sigma^2} \cap \sigma^2| \frac{\partial}{\partial x^q} \Phi_{v_l^{\sigma^2}}^{\sigma^2}, \quad (24)$$

for $k, l, q \in \{0, 1, 2\}$ and (x^0, x^1, x^2) are the ordinary \mathbb{R}^3 coordinates.

3. Curvature approximations

3.1. Curvature vector

The curvature vector \vec{H} is given by

$$\vec{H} = 2H\vec{\nu} \quad (25)$$

for the mean curvature H and normals $\vec{\nu}$. In this paper, the mean curvature is set as the arithmetic mean of the two principal curvatures and H should be all over positive for a sphere (i.e. $H \equiv 1$ on S^2). H and \vec{H} are extrinsic curvature values. This means, that an two dimensional “inhabitant” of the surface can’t determine this kind of curvature in contrast to the Gaussian curvatures. With the inclusion map $\vec{x} := \mathbb{R}^3 \supset M \hookrightarrow \mathbb{R}^3$, which is the position vector of M in \mathbb{R}^3 , the curvature vector can be calculated by (see [5, Ch. 5], [11, Ch. 4.5] or [7])

$$-\Delta_B \vec{x} = \vec{H}. \quad (26)$$

(Note that \vec{x} is an isometric immersion with the common induced metric from \mathbb{R}^3 .)

The equation (26) is to read component-wise and can be discretized with the discrete Laplace-Beltrami operator in (16), where f becomes the i -th coordinate functions x^i for $i = 0, 1, 2$. I.e. we solve for all vertices $v \in K$ and $i = 0, 1, 2$.

$$\langle * \Delta_B x^i, \star v \rangle = \langle * H_{LX}^i, \star v \rangle. \quad (27)$$

$H_{LX}^i \in \mathbb{R}$ are the components of the approximated curvature vector. The right-hand side (RHS) of (27) can be locally represented by the decomposed Voronoi area

$$C_i^{\sigma^2} = |\star v \cap \sigma^2| \quad (28)$$

around $v \prec \sigma^2$. Hence, the local coefficients matrix of the RHS of (27) (and generally for all Zero-Order-Terms of scalar valued functions) becomes

$$\begin{bmatrix} C_0^{\sigma^2} & 0 & 0 \\ 0 & C_1^{\sigma^2} & 0 \\ 0 & 0 & C_2^{\sigma^2} \end{bmatrix} \quad (29)$$

and can be assembly in a common way.

The mean curvature H is determined with (25) by taking the euclidean \mathbb{R}^3 -norm

$$H_{LX} = \frac{s}{2} \left\| \vec{H}_{LX} \right\|_{\mathbb{R}^3} \quad (30)$$

on every vertex with respect to the sign $s : K^{(0)} \rightarrow \{+1, -1\}$, which depends on the direction of \vec{H}_{LX} . If the approximated curvature vector point outward the polytop K , then is $s = +1$ and vice versa.

3.2. Weingarten map

The Weingarten map (shape operator) S can be obtained by rising on time the indices of the second fundamental form II (see [20]), i.e. $S = (g)^{-1} II$ with a metric tensor g , or by the exterior derivatives of the normal components:

$$\begin{aligned} S : T_{\vec{x}} M &\rightarrow T_{\vec{x}} M \\ \vec{w} &\mapsto \mathbf{d}\vec{\nu}(\vec{w}) . \end{aligned} \quad (31)$$

In particularly, $\mathbf{d}\nu^i(\vec{w})$ is the directional derivative of the i -th normal component ν^i along \vec{w} . The eigenvalues of S are the principal curvatures κ_1 and κ_2 . Note that the linear operator S by (31) as matrix have a column space in local coordinates and depends on the choice of the parametrisation as a consequence. A more manageable formulation is the extended Weingarten map

$$\bar{S} := \nabla \vec{\nu}, \quad (32)$$

which can be defined on the entire tangential space of the \mathbb{R}^3 (if the normal vectors of M are smoothly extended to them). The point is, that \bar{S} , restricted to $T_{\vec{x}} M$, is the Weingarten map S (see [14, Pt. 2, Ch. 2]), with the additive eigenvalue 0, and (32) can be approximated by our discrete average gradient (22), i.e. we calculate the i -th row $\bar{s}_i \in \mathbb{R}^3$ of the discrete extended Weingarten map $\bar{S}_W \in \mathbb{R}^{3 \times 3}$ by

$$\langle * \bar{\nabla} \nu^i, \star v \rangle = \langle * \bar{s}_i, \star v \rangle \quad (33)$$

on all vertices $v \in K$. For numerical reason we symmetrize \bar{S}_W by

$$\bar{S}_W^{Sym} := \frac{1}{2} (\bar{S}_W + \bar{S}_W^T) \quad (34)$$

to get the same property like the smooth extended Weingarten map. To obtain the eigenvalues we use the QR-algorithm of the MTL4⁵. The lowest eigenvalue regarding to the absolute value is omitted. So w.l.o.g.

$$\{\kappa_1, \kappa_2\} \approx \{\kappa_{W,1}, \kappa_{W,2}\} \quad (35)$$

$$:= \left\{ \lambda \in \text{Eig}(\bar{S}_W^{Sym}) \mid \exists \lambda_0 \in \text{Eig}(\bar{S}_W^{Sym}) : |\lambda| > \lambda_0 \right\} \quad (36)$$

⁵Matrix Template Library 4

Hence, the approximated Gauss and mean curvatures are

$$K_W := \kappa_{W,1} \cdot \kappa_{W,2} \quad (37)$$

$$H_W := \frac{1}{2} (\kappa_{W,1} + \kappa_{W,2}) . \quad (38)$$

The equations (33) can be applied, only if we know the exact normals of the manifolds on the vertices, e.g. if the surface M is described by the 0-level-set of a signed distance function $\varphi : \mathbb{R}^3 \rightarrow \mathbb{R}$, then is

$$\vec{\nu} = \frac{\nabla_{\mathbb{R}^3} \varphi}{\|\nabla_{\mathbb{R}^3} \varphi\|} . \quad (39)$$

For arbitrary surface triangulations, where the smooth manifold is unknown, like in figure 1, we must approximate the normals on the vertices before. A simple way to do that, is to average the element normals $\vec{\nu}^{\sigma^2}$ of a triangle $\sigma^2 \in K$ over the Voronoi area:

$$\langle * \vec{\nu}_{\text{AvN}}, \star v \rangle := \sum_{\sigma^2 \succ v} |\star v \cap \sigma^2| \vec{\nu}^{\sigma^2} . \quad (40)$$

With these discrete normals on the vertices and the same procedure above, we get then the approximated curvatures $K_{W,\text{AvN}}$ and $H_{W,\text{AvN}}$.

3.3. Gauss-Bonnet-Operator

Thus far, we have two approaches for the mean curvature with sections 3.1 and 3.2. For a second approach of the Gauss curvature, we want to use a Gauss-Bonnet approximation, like in [18] or [21], for comparison reasons.

On the abstract Voronoi cell $\pi(\star v)$ (arise by projecting to the manifold) of a vertex v , it holds the Gauss-Bonnet theorem [3]:

$$\int_{\pi(\star v)} K \mu = 2\pi - \sum_{i=1}^{m_v} \tilde{\beta}_i - \int_{\partial \pi(\star v)} k_g ds . \quad (41)$$

$\mu \in \Omega^2(M)$ is the volume form, k_g the geodetic curvature on the boundary edges of the cell and $\tilde{\beta}_i$ the m_v exterior angles of the boundary on the Voronoi vertices. This can be approximated on the simplicial complex K by omitting the projection. The geodetic curvature k_g vanish on the straight lines and on the bucklings, where the dual edges intersect the primal edges in right angles. Hence, in our DEC notation, we get

$$\langle * K_{GB}, \star v \rangle := 2\pi - \sum_{i=1}^{m_v} \beta_i \quad (42)$$

on a vertex $v \in K$, with the exterior angles β_i . We see in figure 4, that it is possible to calculate the exterior angles by the local interior angles α_0 and α_1 on v for a triangle $\sigma^2 \succ v$:

$$\beta^{\sigma^2} = \pi - \gamma_0 - \gamma_1 = \alpha_0 + \alpha_1 . \quad (43)$$

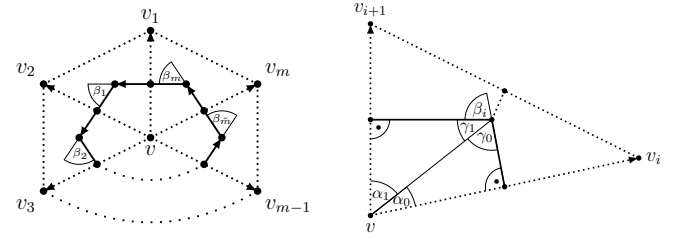


Figure 4: Left: $m = m_v =: \tilde{m} + 1$ exterior angles β_i on the vertices of a Voronoi cell. The solid lines (with orientations) marks the dual (Voronoi) edges. Right: Local angles ($\beta^{\sigma^2} := \beta_i$) in a primal triangle σ^2 referring to the edges of the circumcenter subdivision.

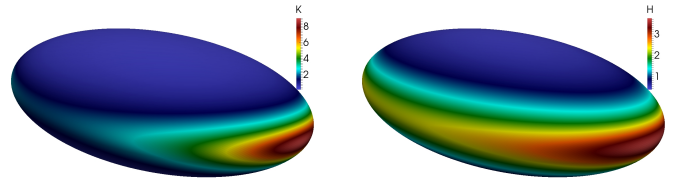


Figure 5: Ellipsoid (46): Gaussian curvature K (left) and mean curvature H (right).

Because the interior angles are determinable by the length measures of the edges, we get

$$\sum_{i=1}^{m_v} \beta_i = \sum_{\sigma^2 \succ v} \sum_{\sigma^2 \succ \sigma^1 \succ v} \text{atan2}(2 |\star \sigma^1 \cap \sigma^2|, |\sigma^1|) \quad (44)$$

for the angle sum in (42).

4. Results

4.1. Test surfaces

For our numerical tests, we use the following 4 surfaces, with analytical known Gauss and mean curvatures:

Sphere (unit) with given signed distance function

$$\varphi(x, y, z) := x^2 + y^2 + z^2 - 1 . \quad (45)$$

The Gauss and mean curvature are all over 1 on the unit sphere.

Ellipsoid (tri-axial; length of semi-principal axes: (1, 0.5, 1.5)) with given signed distance function

$$\varphi(x, y, z) := (3x)^2 + (6y)^2 + (2z)^2 - 9 \quad (46)$$

and curvatures (see Figure 5)

$$K(x, y, z) = \frac{11664}{(81 + 972y^2 - 20z^2)^2} \quad (47)$$

$$H(x, y, z) = \frac{36(45 + 54y^2 - 10z^2)}{(81 + 972y^2 - 20z^2)^{3/2}} . \quad (48)$$

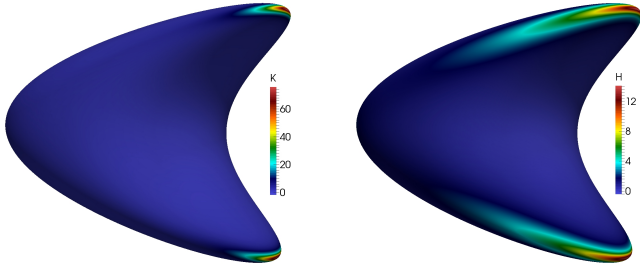


Figure 6: Quartic surface(49): Gaussian curvature K (left) and mean curvature H (right).

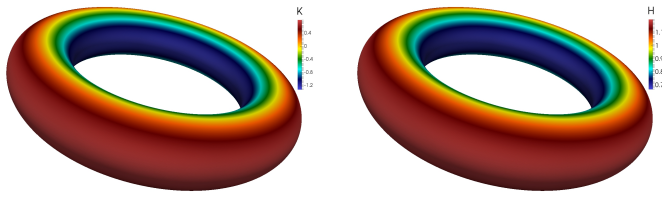


Figure 7: Torus (52): Gaussian curvature K (left) and mean curvature H (right).

Quartic surface with given signed distance function

$$\varphi(x, y, z) := (x - z^2)^2 + (y - z^2)^2 + z^2 - 1 \quad (49)$$

and curvatures (see Figure 6)

$$K(x, y, z) = -\frac{1 + 2x - 2x^2 + 2y - 2y^2 + 2(-3 + x + y)z^2}{1 - 4(-2 + x + x^2 + y - 2xy + y^2)z^2} \quad (50)$$

$$H(x, y, z) = -\frac{x - x^2 + y - y^2 + (-7 + 3x + 3y)z^2}{1 - 4(-2 + x + x^2 + y - 2xy + y^2)z^2}. \quad (51)$$

Torus with major radius⁶ $R = 2$ and minor radius⁷ $r = 0.5$ with given signed distance function

$$\varphi(x, y, z) := \left(2 - \sqrt{x^2 - y^2}\right)^2 + z^2 - 0.25 \quad (52)$$

and curvatures (see Figure 7)

$$K(x, y, z) = 4 - \frac{8}{\sqrt{x^2 + y^2}} \quad (53)$$

$$H(x, y, z) = 2 - \frac{2}{\sqrt{x^2 + y^2}}. \quad (54)$$

4.1.1. Notes on meshing

Except for the torus, all macro triangulations are icosahedrons. In [19], we see that the 20 plane faces are able to divide in N^2 equal equilateral triangles and all vertices can projected to the smooth surface. Unfortunately, this

procedure doesn't results in a well-centered simplicial complex for the ellipsoid and the quartic surface. Our resort for this problem provide a mechanical evolution for the coordinates \vec{x}_i of the vertices $v_i \in K$

$$\frac{d\vec{x}_i}{dt} = \vec{F}(\vec{x}_i). \quad (55)$$

The force vector $\vec{F}(\vec{x}_i)$ describe the interaction with the adjoining edges $\sigma^1 \succ v_i$ and triangles $\sigma^2 \succ v_i$. We use two approaches for \vec{F} , who will linear combined. One is to displace the vertices, so that all edges grasp at the same length. This is similar to a overlapping sphere (OS)/ Voronoi tesselation (VT) hybrid model in [17], with fixed connectivity, for simulating the arrangement of cells in tissue. The other approach is to choose \vec{F} so, that the edges $\sigma^1 \succ v_i$ will become longer or shorter in dependency of the enclosed angle of σ^1 and the other edge $\tilde{\sigma}^1 \prec \sigma^2$ on all triangles $\sigma^2 \succ v_i$. The aspired optimum (which can't be reached in general) can be a enclosed angle of $\frac{\pi}{3}$ for example.

The equation (55) can be numerical solved by the explicit Euler method. It must be pointed out, that the smooth surface M gives us a geometrical constrain for the coordinates \vec{x}_i . That's why we project all vertices to M after every Euler step. A explicit base method of higher order doesn't result in faster convergence in practice because of the projection and a implicit method is hard to implement with all of the dependencies of \vec{F} in mind.

The torus mesh in figure 7 can be obtain by a uniform triangulation of a tube and glue the both ends together with a twist of 4π along the tube. The meshes for the bunny and the horse in figure 1 are produced with the great AVCD⁸ remeshing tool (see [22]) with some hand-made corrections (clearing up the few 1-rings with less than 5 triangles).

4.2. Comparing method

For the three test surfaces of genus 0 (sphere, ellipsoid, quartic surface) exists experimental results in [12] by C-J. Heine. There is a isoparametric finite element approach deployed of degree 1 till 4 for the approximation of the curvatures. We only want to use the results of the degree 2 FE-Method (FEM-D2) to compare with our calculations, because the linear FEM-D1, which is the only really comparable with regard to the computation effort, is not convergent and FEM-D3, resp. FEM-D4, is too expensive in contrast to our methods. The lack of convergence of the discrete curvature vector with a linear FEM is discussed in [4]. The advantage of a FE approach is that the triangulation doesn't need to be well-centered. Therefore, the global mesh refinement strategy in [12] is to bisect the longest edge of a triangle. This produce triangulations of 1-rings with 4 or 8 elements in about equal parts, i.e. the average are approximately 1-rings with 6 elements like

⁶distance from the center of the tube to the center of the torus

⁷radius of the tube

⁸Approximated Centroidal Voronoi Diagram

Method	GB	LX	W	W,AvN	FEM-D1	FEM-D2	FEM-D3	FEM-D4
IDOFs	3	9	27	36	36	72	120	180

Table 1: IDOFs for different methods in ascending order. Our 4 approaches and the FEM-D2 from [12] for comparing are highlighted gray

our triangulations (all 1-rings have 6 elements, except the 12 defects with 5 triangles). That's the reason, why the number of local DOFs (IDOFs) per triangle is a plausible measurement for the relative costs to compare the FE and DEC methods. E.g. for one value on a global vertex with 6 adjacent elements and a linear method (i.e. local coefficients matrix in $\mathbb{R}^{3 \times 3}$) we get a row with 7 NNZ⁹ in the assembled global coefficients matrix independently of the choice of the method. For the calculation of the DEC-discretized curvature vector (LX) with (27), we have to solve the Laplace-Beltrami for the 3 components of the position vector on every vertices. Therefor, there are 9 IDOFs on every triangle element. For the Weingarten map approach (W) with (33), we must calculate a 3×3 -matrix on a vertex ($\Rightarrow 27$ IDOFs). If the normals are unknown (W,AvN), then 3 IDOFs are added per vertex ($\Rightarrow 36$ IDOFs). The Gauss-Bonnet approximation gives us only 3 DOFs per vertex ($\Rightarrow 9$ IDOFs). In the FE-approaches (FEM-D*) in [12] is the Weingarten map and the curvature vector, as interim result, to be calculated. But at this, is to respect the growing number of DOFs per value with higher degrees of the elements. A summary is displayed in table 1.

4.3. Numerical experiments

We have implemented all curvature approximation approaches of section 3 in a AMDiS framework. So we defined only the (triangle) element coefficients matrix as element operators and used linear functions for the interpolation of the results. The solving of the resulting linear system was done by the BiCGStab¹⁰. Like in [12], the errors were measured in the discrete relative L_r -norm ($r \in \{2, \infty\}$), i.e. the absolute errors were globally normalized by the norm of the analytical solutions:

$$\text{Err}_r := \frac{\|C - C_{\text{Meth}}\|_{L_r(|K|)}}{\|C\|_{L_r(|K|)}}. \quad (56)$$

$C \in \{K, H\}$ is the curvature value and "Meth" the used method. For $r = 2$ we plot the errors for our test surfaces in figures 8, 10, 12 and 13 in a log-scale on both axis. The axis of abscissas describe the fineness of the triangulation and is measured in

$$h := 2 \max_{\sigma^2 \in K} \left\| \vec{x}(v^{\sigma^2}) - \vec{x}(\star\sigma^2) \right\|_2, \quad (57)$$

with an arbitrary vertex $v^{\sigma^2} \prec \sigma^2$, i.e. h is the maximum over all circumscribed diameters. We see in table

⁹Number of NonZero elements

¹⁰BiConjugate Gradient Stabilized method with $l = 2$

2 the EOCs (Experimental Order of Convergence) for the both lowest h in the appropriate norm. The reason for the choice of the finest meshes is the sometimes poor resolution of coarser triangulations. E.g. we see, by the mean of the slope, no or only lower convergence at mounted h for the quartic surface in figure 12, because the mesh don't picture good enough the two ridges, so that the geometrical error exceeds the error of the method. In general, it is often to observe, that there is a kind of "transient phase" with respect to the order of convergence. And the higher the "complexity" of the surface the longer is this phase.

However, on the sphere and the ellipsoid stagnate the EOCs for the discrete maximum norm on finer triangulations. In figure 9 and 11 (top) we see that maximum errors sticks on the defects of the hexagonal mesh structure for the W, AvN methods respectively for K_{GB} . Figure 11 (bottom) point to a similar error behavior for calculation of the curvature vector on the ellipsoid, but there are larger errors on the outer vertices of the 1-rings too.

4.4. Conclusion

With regard to the errors and the computational effort, the Gauss-Bonnet-Operator for the Gauss curvature (K_{GB}) and the curvature vector with the DEC-discretized Laplace-Beltrami-Operator for the mean curvature (H_{LX}) seems to be the best choice of method for our used examples. But the advantage of the calculation of the Weingarten map is the higher information content, because W gives us the whole shape-operator and the both principal curvatures as consequence and hence W must be only one time calculated to get K and H simultaneous.

Table 2 leads to guess of a nearly second order method for the DEC-discretized Weingarten map (W) if the normals of the smooth surface are known on every vertex. This partially not hold if the normals are averaged over the adjacent element normals (W, AvN). So that a better approximation of the vertex normals can maybe leads to a better order of convergence up to 2.

References

- [1] Abraham, R., Marsden, J., Ratiu, T., 1988. Manifolds, Tensor Analysis, and Applications. No. Bd. 75 in Applied Mathematical Sciences. Springer New York.
- [2] Bell, N., Hirani, A. N., Nov. 2012. Pydec: Software and algorithms for discretization of exterior calculus. ACM Trans. Math. Softw. 39 (1), 3:1–3:41.
URL <http://doi.acm.org/10.1145/2382585.2382588>
- [3] Berger, M., Gostiaux, B., 1988. Differential geometry: manifolds, curves, and surfaces. Graduate texts in mathematics. Springer-Verlag.
URL <http://books.google.de/books?id=CKWodhkU-Y0C>

EOC	Sphere				Ellipsoid				Quartic surface				Torus			
	K		H		K		H		K		H		K		H	
	L_2	L_∞	L_2	L_∞	L_2	L_∞	L_2	L_∞	L_2	L_∞	L_2	L_∞	L_2	L_∞	L_2	L_∞
GB(K) / LX(H)	2.0	2.0	2.4	1.7	1.4	NC	1.9	NC	1.8	1.8	1.8	1.8	1.9	1.0	1.9	1.4
W	2.0	2.0	2.0	2.0	2.0	2.0	2.0	2.0	1.7	1.8	1.8	1.8	2.0	2.1	2.0	2.0
W,AvN	1.4	NC	1.4	NC	1.9	NC	2.0	NC	1.6	1.6	1.7	1.6	2.0	2.1	2.0	2.0
FEM-D2	2.4	2.0	2.4	2.0	1.3	1.7	1.1	1.3	2.0	2.2	1.4	1.4				

Table 2: Experimental Order of Convergence (EOC) of both finest triangulations for the relative discrete L_2 - and L_∞ -norm. Values lower than 0.1 are denoted as NC (No Convergence).

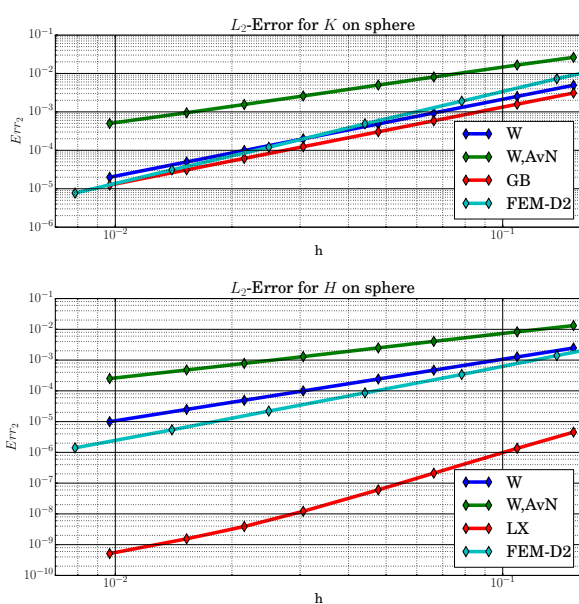


Figure 8: Sphere (45): Relative L_2 error for K (top) and H (bottom) for different h in a log-log-plot.

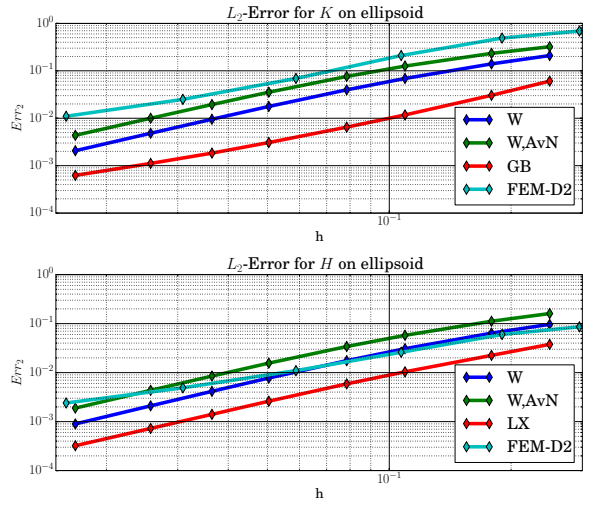


Figure 10: Ellipsoid (46): Relative L_2 error for K (top) and H (bottom) for different h in a log-log-plot.

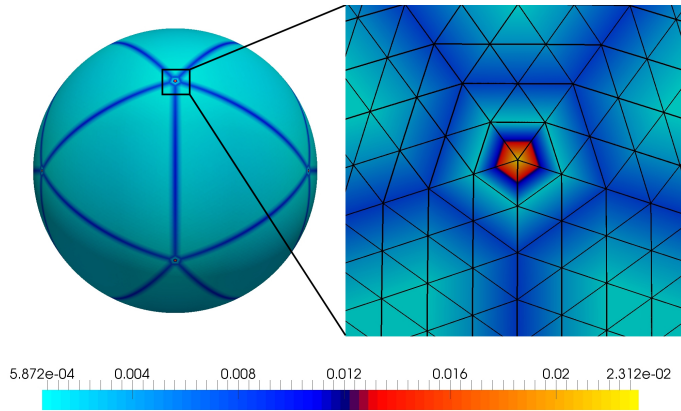


Figure 9: Sphere (45): The maximal errors for $K_{W,AvN}$ keeps on the 12 vertices with 1-rings of 5 triangles. 25002 DOFs were used ($h \approx 0.03$). The errors for $H_{W,AvN}$ results in a similar picture.

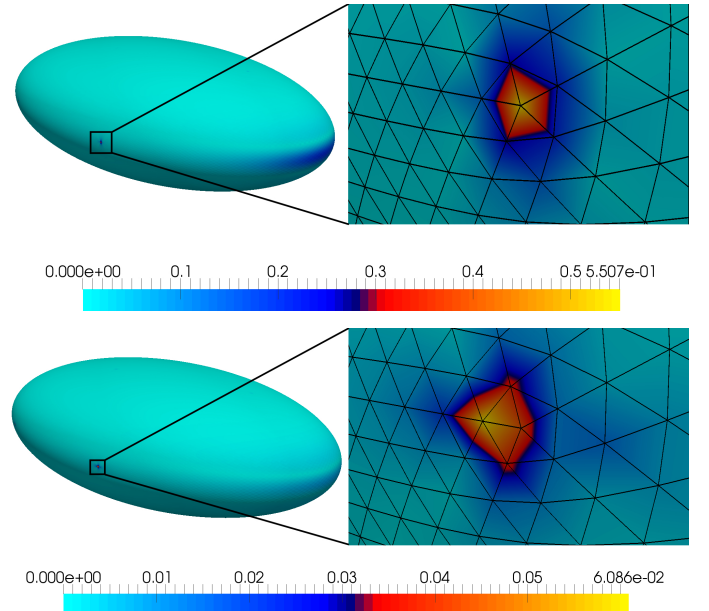


Figure 11: Ellipsoid (46): The maximal errors for $K_{W,AvN}$ (top) keeps primarily on the lateral 4 of all 12 vertices with 1-rings of 5 triangles. The errors for K_{GB} and $H_{W,AvN}$ results in a similar picture. Slightly different is the situation at the errors for H_{LX} (bottom). There are the maximums partially on vertices in the neighbourhood. 100002 DOFs were used ($h \approx 0.026$).

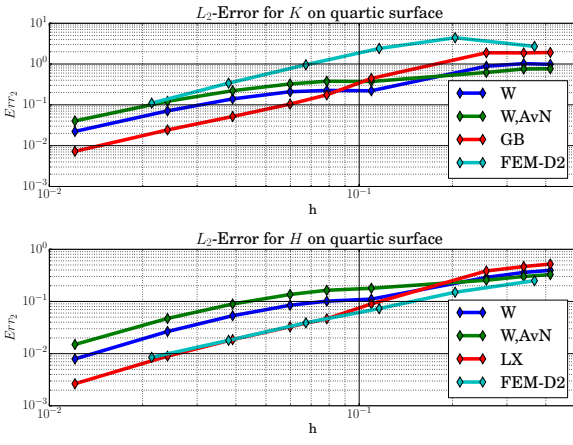


Figure 12: Quartic surface (49): Relative L_2 error for K (top) and H (bottom) for different h in a log-log-plot.

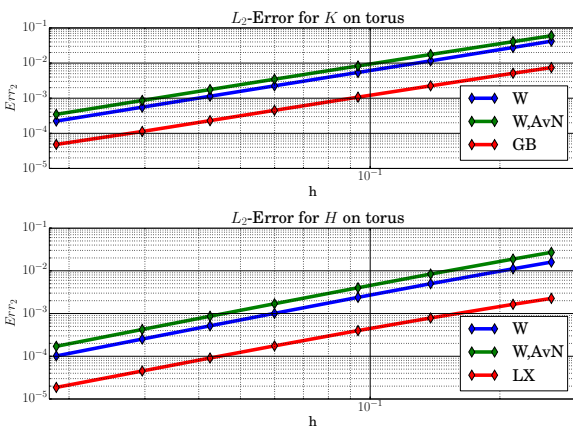


Figure 13: Torus (52): Relative L_2 error for K (top) and H (bottom) for different h in a log-log-plot.

- [4] Bonito, A., Nochetto, R., Pauletti, M., 2010. Geometrically consistent mesh modification. SIAM Journal on Numerical Analysis 48 (5), 1877–1899.
URL <http://dx.doi.org/10.1137/100781833>
- [5] Chen, B., 1984. Total Mean Curvature and Submanifolds of Finite Type. Pure Mathematics Series. World Scientific.
URL <http://books.google.de/books?id=w6p21v3AGy0C>
- [6] Crane, K., de Goes, F., Desbrun, M., Schröder, P., 2013. Digital geometry processing with discrete exterior calculus. In: ACM SIGGRAPH 2013 Courses. SIGGRAPH '13. ACM, New York, NY, USA, pp. 7:1–7:126.
URL <http://doi.acm.org/10.1145/2504435.2504442>
- [7] Deckelnick, K., Dziuk, G., Elliott, C. M., 5 2005. Computation of geometric partial differential equations and mean curvature flow. Acta Numerica 14, 139–232.
URL http://journals.cambridge.org/article_S0962492904000224
- [8] Desbrun, M., Hirani, A. N., Leok, M., Marsden, J. E., Aug. 2005. Discrete Exterior Calculus. ArXiv Mathematics e-prints.
- [9] Desbrun, M., Kanso, E., Tong, Y., 2005. Discrete differential forms for computational modeling. In: ACM SIGGRAPH 2005 Courses. SIGGRAPH '05. ACM, New York, NY, USA.
URL <http://doi.acm.org/10.1145/1198555.1198666>
- [10] Elcott, S., Schröder, P., 2005. Building your own dec at home. In: ACM SIGGRAPH 2005 Courses. SIGGRAPH '05. ACM, New York, NY, USA.
URL <http://doi.acm.org/10.1145/1198555.1198667>
- [11] Flanders, H., 1963. Differential Forms with Applications to the Physical Sciences. Dover books on advanced mathematics. Dover Publications.
URL <http://books.google.de/books?id=pGOP11I008kC>
- [12] Heine, C.-J., 2004. Isoparametric finite element approximation of curvature on hypersurfaces. Preprint Fak. f. Math. Phys. Univ. Freiburg (26).
- [13] Hirani, A. N., 2003. Discrete exterior calculus. Ph.D. thesis, California Institute of Technology, Pasadena, CA, USA, aAI3086864.
- [14] Kimura, M., Laurençot, P., Yazaki, S., Beneš, M., Feireisl, E., fyzikální fakulta, U. K. M., 2008. Topics in Mathematical Modeling. Nečas Center for Mathematical Modeling: Lecture notes. Matfyzpress.
URL <http://books.google.de/books?id=DbZRQwAACAAJ>
- [15] Meyer, M., Desbrun, M., Schröder, P., Barr, A., 2003. Discrete differential-geometry operators for triangulated 2-manifolds. In: Hege, H.-C., Polthier, K. (Eds.), Visualization and Mathematics III. Mathematics and Visualization. Springer Berlin Heidelberg, pp. 35–57.
URL http://dx.doi.org/10.1007/978-3-662-05105-4_2
- [16] Nitschke, I., 2014. Diskretes Äußeres Kalkül (DEC) auf Oberflächen ohne Rand. Diploma thesis, TU Dresden - Department of Mathematics.
- [17] Pathmanathan, P., Cooper, J., Fletcher, A., Mirams, G., Murray, P., Osborne, J., Pitt-Francis, J., Walter, A., Chapman, S. J., 2009. A computational study of discrete mechanical tissue models. Physical Biology 6 (3), 036001.
URL <http://stacks.iop.org/1478-3975/6/i=3/a=036001>
- [18] Polthier, K., Schmies, M., 2006. Straightest geodesics on polyhedral surfaces. In: ACM SIGGRAPH 2006 Courses. SIGGRAPH '06. ACM, New York, NY, USA, pp. 30–38.
URL <http://doi.acm.org/10.1145/1185657.1185664>
- [19] Sadourny, R., Arakawa, A., Mintz, Y., Jun. 1968. Integration of the nondivergent barotropic vorticity equation with an icosahedral-hexagonal grid for the sphere1. Monthly Weather Review 96 (6), 351–356.
URL [http://dx.doi.org/10.1175/1520-0493\(1968\)096%3C0351:iotnbv%3E2.0.co;2](http://dx.doi.org/10.1175/1520-0493(1968)096%3C0351:iotnbv%3E2.0.co;2)
- [20] Shifrin, T., 2014. Differential Geometry: A First Course in Curves and Surfaces. University of Georgia.
- [21] Surazhsky, T., Magid, E., Soldea, O., Elber, G., Rivlin, E., 2003. A comparison of gaussian and mean curvatures estimation methods on triangular meshes. In: ICRA. pp. 1021–1026.

- [22] Valette, S., Chassery, J.-M., 2004. Approximated centroidal voronoi diagrams for uniform polygonal mesh coarsening. Computer Graphics Forum 23 (3), 381–389.
URL <http://dx.doi.org/10.1111/j.1467-8659.2004.00769.x>
- [23] Witkowski, T., Voigt, A., May 2010. A multi-mesh finite element method for Lagrange elements of arbitrary degree. ArXiv e-prints.
- [24] Xu, G., 2004. Discrete laplace–beltrami operators and their convergence. Computer Aided Geometric Design 21 (8), 767 – 784, geometric Modeling and Processing 2004.
URL <http://www.sciencedirect.com/science/article/pii/S0167839604000810>